

Supplementary Information:

Template-Directed 2D Nanopatterning of $S=1/2$ Molecular Spins

Kyungju Noh^{a,b}, Luciano Colazzo^{,a,c}, Corina Urdaniz^{a,c}, Jaehyun Lee^{a,b}, Denis Krylov^{a,c}, Parul Devi^{a,c}, Andrin Doll^d, Andreas J. Heinrich^{a,b}, Christoph Wolf^{*,a,b}, Fabio Donati^{*,a,b}, Yujeong Bae^{*,a,b}*

^aCenter for Quantum Nanoscience (QNS), Institute of Basic Science (IBS), 03760 Seoul, Republic of Korea

^bDepartment of Physics, Ewha Womans University, 03760 Seoul, Republic of Korea

^cEwha Womans University, 03760 Seoul, Republic of Korea

^dSwiss Light Source (SLS), Paul Scherrer Institut (PSI), 5232 Villigen, Switzerland

Contents

1 Methods

- 1.1 Sample Preparation
- 1.2 Scanning Tunneling Microscopy
- 1.3 X-ray Adsorption Spectroscopy
- 1.4 Multiplet Calculations
- 1.5 Density Functional Theory Calculations

2 Adsorption Geometry

- 2.1 Geometric Structure of TiOPc Monolayer
- 2.2 Geometric Structure of VOPc on TiOPc Monolayer
- 2.3 Geometric Structure of TiOPc on TiOPc Monolayer

3 Additional X-ray Absorption Data and Multiplet Calculations

- 3.1 Background Subtraction Procedure
- 3.2 Details of Multiplet Calculations

3.3 Additional X-ray Data

4 Additional dI/dV Spectra and DFT Calculations

1. Methods

1.1 Sample Preparation

The Ag(100) substrate was prepared in ultra-high vacuum (UHV) by repeated cycles of Ar sputtering at 5.0×10^{-6} Torr and annealing at 700 K until an atomically flat surface with large terraces was observed via STM. TiOPc (99% purity) and VOPc (90% purity) were purchased from Sigma-Aldrich and used without further purification. Before deposition, the molecules were thermally degassed at 620 K for several hours in the UHV chamber. VOPc was sublimated at the crucible temperature of 593 K, and TiOPc was sublimated at 609 K using a homebuilt Knudsen cell evaporator. The silver substrate was kept at room temperature during the molecular deposition. To calculate the coverage of bilayer system, the 2nd layer coverage was calculated by dividing the number of 2nd layer molecules with the number of 1st layer molecules in the same area, estimated from the density of 1st layer molecules on Ag(100). To obtain the highly ordered structure of VOPc, post-annealing was performed at $T_{\text{Ag}} = 540$ K. The substrate temperature while annealing was measured using pyrometers for the STM and X-ray experiments. The temperature required to observe the long-range order differs between the two systems by $\sim 9.1\%$. In the main text, we indicate the temperature calibrated according to the STM system.

1.2 Scanning Tunneling Microscopy

STM experiments were performed by using a pan-type scan head (RHK PanScan Freedom) at 10 K with a base pressure of 5.0×10^{-11} mbar. All STM measurements were carried out with a Pt-Ir tip (Pt 80 %, Ir 20 %). Topography and dI/dV maps were recorded in constant current mode and the dI/dV curves were measured in constant height mode, by using a digital lock-in amplifier with a modulation bias voltage of 15 mV and a frequency of 908 Hz.

1.3 X-ray Absorption Spectroscopy

XAS, XMCD, and XLD measurements of VOPc/TiOPc molecular layers on Ag(100) were performed at the EPFL-PSI X-treme beamline.¹ The samples were prepared *in situ* with the method explained above and characterized prior to the X-ray experiments using a Omicron VT-STM available at the beamline. The sample was transferred from the preparation chamber to the XAS measurement stage without breaking the vacuum. The measurements were

performed at 300 K and 2.5 K and at magnetic fields of up to 6.8 T. Circularly and linearly polarized light from the synchrotron source was directed on the sample with the photon beam parallel to the magnetic field either at normal or at grazing (60°) incidence. The circular right (C^+) and left (C^-) photon polarizations are defined with respect to the photon beam direction while the linear horizontal (L^H) and vertical (L^V) photon polarizations are defined with respect to the sample surface, as sketched in the inset of Fig. 2a and 2c. All signals have been acquired in total electron yield and normalized at the related pre-edge intensity. Background spectra over the energy range of the V $L_{2,3}$, Ti $L_{2,3}$, C K, and N K edges were acquired on a clean Ag(100), normalized to the absorption at the related pre-edge energy, and subtracted from the spectra of samples covered with the molecular films (see section 3.1 for more details on the background subtraction procedure). In all plots, the XAS units indicate the relative edge jump with respect to the pre-edge absorption.

1.4 Multiplet Calculations

X-ray spectra of V $L_{2,3}$ edges were simulated using the Quanty multiplet code² including electron-electron interaction, spin-orbit coupling, crystal field splitting of the $3d$ orbitals, and Zeeman interaction. Values of the Slater integrals and spin-orbit coupling were obtained using atomic calculations with the Cowan code.³ Rescaling factors for the $3d-3d$ and $2p-3d$ Slater integrals, as well as the relative on-site energy of the $3d$ orbitals were used as free parameters to fit the experiments. The fit was performed using a Bayesian optimization algorithm over a set of angular dependent circular and linear absorption spectra and minimizing the sum of the individual mean square error of each spectrum (Fig. S3). To compensate for the different intensities of the spectra in the error calculation, we assign a weight of ten to one to the error values of the XMCD and XLD compared to those of the XAS spectra. We used 2 independent parameters for the electron-electron interaction and 3 independent parameters for the on-site orbital energy, plus an additional overall amplitude scaling factor to match the calculation and experimental intensities. The spectra were calculated taking the imaginary part of the Green functions of the electric dipole transition operator applied to the vanadium electron wavefunctions⁴ with a Lorentzian broadening of 70 meV to match the linewidth of the lowest energy X-ray transitions. To reproduce the energy dependent life-time of the X-ray absorption excitation,⁵ we further applied a linear photon energy-dependent gaussian broadening

ranging from 0.01 eV to 1.1 eV over the V L_{2,3} spectra energy range. The best value obtained from the fit are shown in Table S1.

1.5 Density Functional Theory Calculations

We performed DFT calculations using plane-wave basis and pseudopotentials as implemented in Quantum Espresso (V6.8 and V7.0).^{6, 7} We used projector augmented-wave (PAW) pseudopotentials from the PSLibrary.⁸ The exchange-correlation was approximated using the PBE functional,⁹ and dispersive forces were treated using the revised VV10 method (rvv10).¹⁰ We note that the choice of the van der Waals correction mostly affects the interaction between molecules and the metal surface, whilst having relatively little impact on the molecules themselves.

All cells were built by creating suitable lateral supercells of the relaxed simple unit cells and padded in z-direction with ~1.5 nm of vacuum as well as decoupled from the periodic images in z-direction by using dipole correction. Cutoffs for the energy and charge density were chosen at 80 Ry and 640 Ry, respectively, and integration of the Brillouin zone was performed using only the Gamma point. In all calculations we applied a Hubbard U correction on the transition metal core of the molecules to improve the description of the localized 3d states and restores the correct orbital order in the case of VOPc. A value of U = 3.6 eV on Ti 3d results in a HOMO-LUMO gap of ~1.5 eV between C π and π^* states, which is in excellent agreement with a previous report.¹¹ For VOPc, we find a similar HOMO-LUMO gap of ~1.6 eV for any value of U > 2.1 eV on the V 3d states, and we therefore used the value of U = 2.1 eV for the shown calculations. All simulated STM images and dI/dV curves were obtained using STMpw¹² in its most recent version.¹³

2. Adsorption Geometry

2.1 Geometric Structure of TiOPc Monolayer

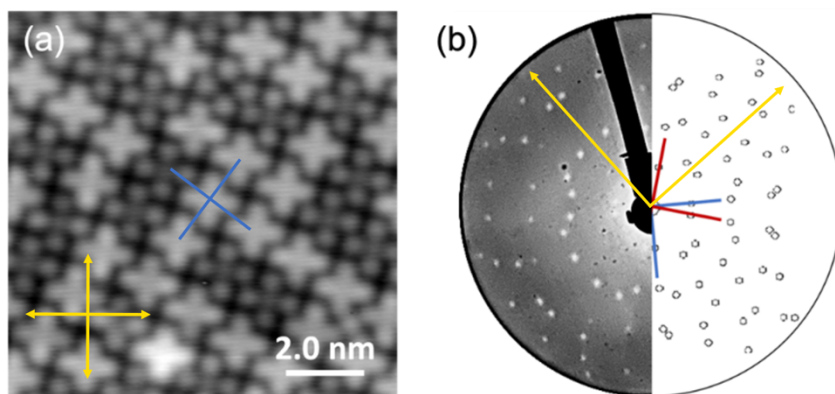


Figure S1. (a) STM image of the TiOPc monolayer on Ag(100) (scan parameters: $V_{DC} = 100$ mV, $I_{set} = 50$ pA) with overlay of molecular unit cell vector (blue lines) and Ag(100) substrate main directions (yellow arrows). (b) LEED pattern collected at room temperature (electron beam energy of 35 eV) and overlaid LEED pattern simulation. Reciprocal space unit vectors for the two subsets of symmetry equivalent TiOPc domains (red and blue) and the Ag(100) substrate (yellow).

In order to characterize TiOPc lattice periodicity and to obtain its unit cell parameters, we performed a combined STM and LEED investigation on a closely packed 0.85 ML TiOPc as-deposited on Ag(100). Via STM we observe that the TiOPc molecules form differently oriented molecular domains on the surface. By selecting one of them (Fig. S1a) we obtain molecular lattice vectors $a = 1.2 \pm 0.1$ nm and $b = 1.2 \pm 0.1$ nm, with an angle of 89 ± 1 degrees between them. The STM measurements reveal that the molecules arrange in a nearly square unit cell rotated by 37 ± 1 degrees with respect to the main directions of the underlying Ag(100) substrate. It is worth to point out that STM measurements can be easily affected by temperature fluctuations during the measurements and further systematic error intrinsic to the measurement.

The diffraction patterns obtained by LEED measurements (Fig. S1b, left), on the same sample, reveal clear spots due to an ordered molecular superstructure and its complexity supports the STM observation that the self-assembled molecular layers arrange with multiple sets of symmetry equivalent domains. We simulated the LEED pattern (Fig. S1b, right) with a

superlattice characterized by the epitaxial matrix $(4, -3 \mid 3, 4)$ associated with 2 subsets of 4 symmetry equivalent domains individually rotated by ± 37 degrees (see blue and red unit vectors in Fig. S1c) with respect to the underlying substrate. Each domain is characterized by a square unit cell with lattice vectors $a^1 = 1.44$ nm, in good agreement with our STM measurements.

2.2 Geometric Structure of VOPc on TiOPc Monolayer

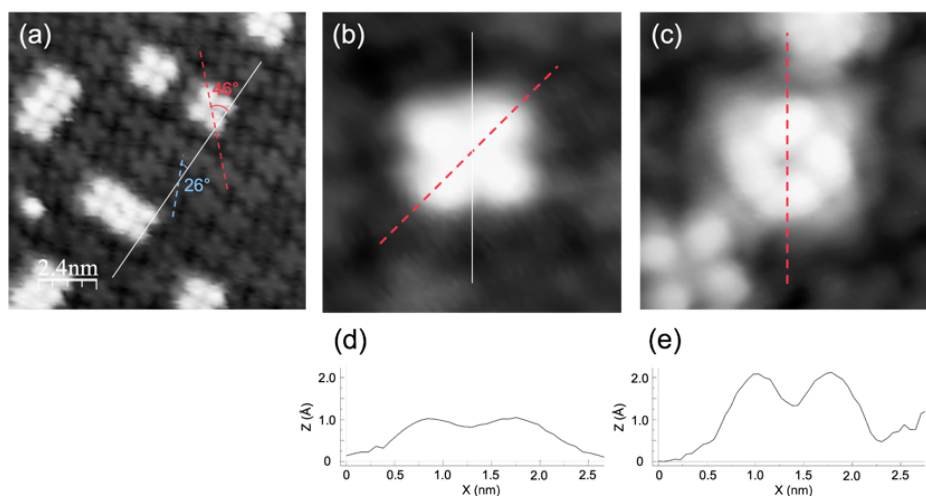


Figure S2. Azimuthal angle of VOPc^A and VOPc^B. (a) STM image of the VOPc^A on TiOPc monolayer (scan size: $12 \times 12 \text{ nm}^2$, $V_{\text{DC}} = 100 \text{ mV}$, $I_{\text{set}} = 50 \text{ pA}$). The white, blue, and red lines represent the molecular unit cell vector direction, the TiOPc lobe direction in the 1st layer, and the VOPc lobe direction in the 2nd layer, respectively. (b) STM images showing the azimuthal angle of VOPc^A and (c) VOPc^B with respect to the molecular unit cell vector direction. In (c), the white line is overlapped with the red line. (d,e) Line profiles over the dashed red line indicated in (b) and (c), respectively [(b): scan size: $3.4 \times 3.4 \text{ nm}^2$, $V_{\text{DC}} = 400 \text{ mV}$, $I_{\text{set}} = 50 \text{ pA}$, (c): scan size: $3.4 \times 3.4 \text{ nm}^2$, $V_{\text{DC}} = 50 \text{ mV}$, $I_{\text{set}} = 30 \text{ pA}$].

Here, we characterize the relative azimuthal angles between VOPc^A, VOPc^B, TiOPc, and the molecular unit cell vector using STM topographic images. The molecular directions, defined as the direction of one of the four lobes from in-gap topography, are marked as dotted lines (blue: TiOPc, red: VOPc^{A,B}). The relative angle between the molecular unit cell vector and the lobe direction of TiOPc molecule is measured as 26 ± 2 degrees, and the angle between VOPc^A (red line in Fig. S2(b)) and the molecular unit cell vector (white line in Fig. S2(b)) is measured as 46 ± 3 degrees. In the meanwhile, the molecular direction of VOPc^B is identical to the molecular unit cell vector (Fig. S2c), 46 degrees rotated with respect to the one of VOPc^A.

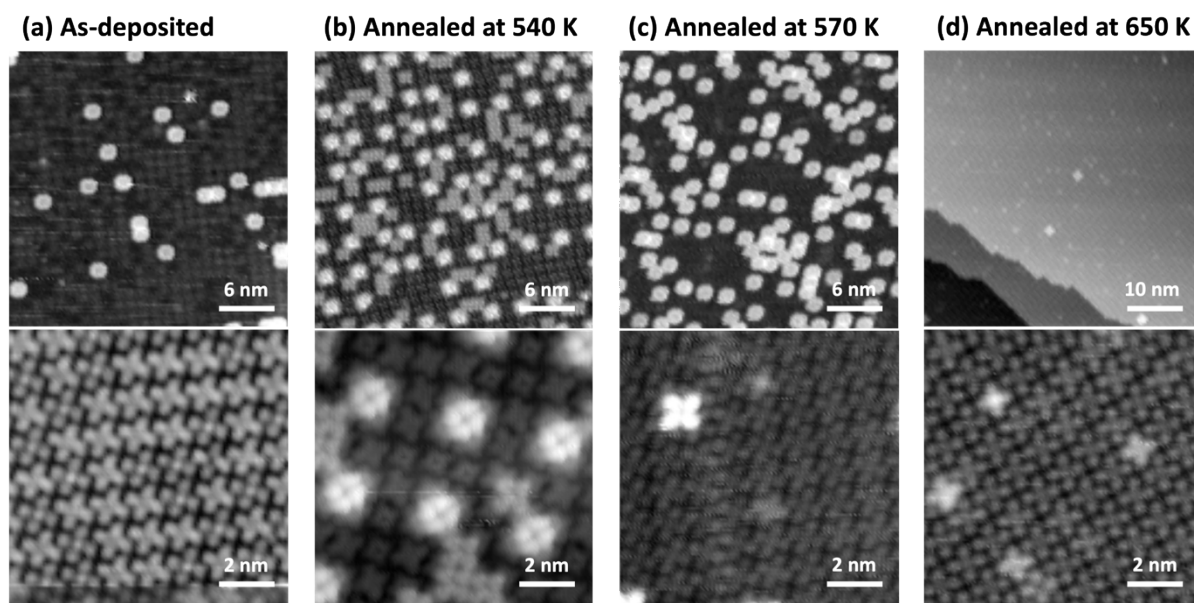


Figure S3. Post annealing temperature dependence of molecular array formation and the 1st layer molecule's adsorption configuration. STM images of low-coverage VOPc on TiOPc layer which is (a) as-deposited, or post annealed at (b) 540 K, (c) 570 K, and (d) 650 K. Scan parameters: (a) upper: $V_{DC} = 1$ V, $I_{set} = 100$ pA; lower: $V_{DC} = 500$ mV, $I_{set} = 100$ pA, (b) upper: $V_{DC} = 50$ mV, $I_{set} = 50$ pA; lower: $V_{DC} = 100$ mV, $I_{set} = 100$ pA, (c) upper: $V_{DC} = 1$ V, $I_{set} = 100$ pA; lower: $V_{DC} = 100$ mV, $I_{set} = 100$ pA, (d) upper: $V_{DC} = 100$ mV, $I_{set} = 70$ pA; lower: $V_{DC} = 100$ mV, $I_{set} = 100$ pA.

In Fig. S3, we show the evolution of VOPc/TiOPc system in various post-annealing temperatures. For the as-deposited sample (Fig. S3a), the 2nd layer molecules are only composed with VOPc^A, and in the 1st layer, TiOPc molecules have 1:1 ratio of O-up and O-down configuration. After annealing at 540 K (Fig. S3b), we observe well organized arrays of VOPc^B, as well as VOPc^A randomly distributed in between VOPc^B arrays. The 1st layer molecules still has 1:1 ratio of O-up and O-down. After post-annealing at even higher temperature (570 K, Fig. S3c), VOPc^B is vanished, and only VOPc^A is observed. The molecule's population remains the same, suggesting that VOPc^B molecules are turned back into VOPc^A type rather than that the B-type molecules are desorbed. The lower panel of (c) shows that O-up configuration is dominating in the 1st layer after annealing at 570 K. Finally, after annealing at 650 K (Fig. S3d), the second layer molecules are desorbed.

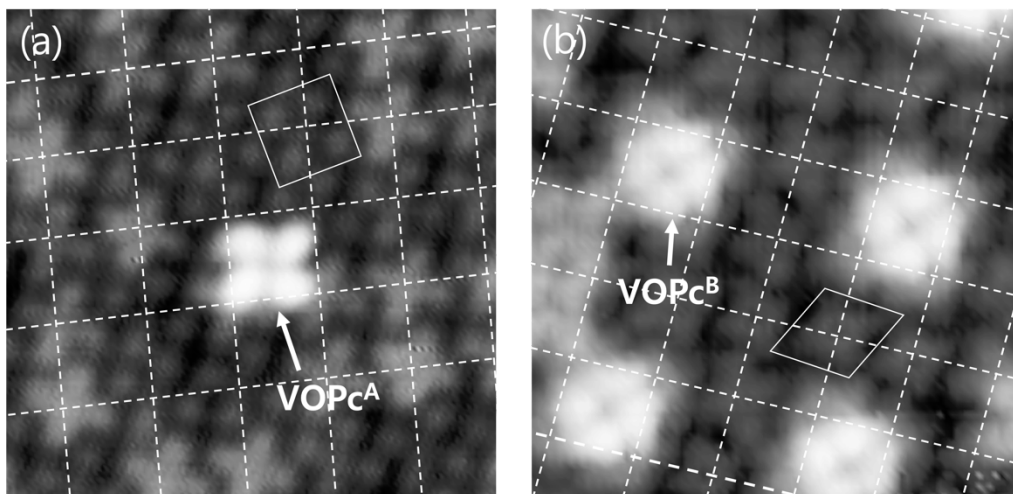


Figure S4. High-resolution STM images showing the 1st layer TiOPc molecules under the 2nd layer VOPc molecules. (a) The 1st layer TiOPc molecules around the 2nd layer VOPc^A molecule (scan parameters: $V_{DC} = 400$ mV, $I_{set} = 50$ pA, $T = 10$ K, scan size: 7×7 nm²) (b) The 1st layer TiOPc molecules around the 2nd layer VOPc^B molecule (scan parameters: $V_{DC} = 50$ mV, $I_{set} = 30$ pA, $T = 10$ K, scan size: 7×7 nm²)

Figure S4 compares the geometry of the 1st layer TiOPc molecules around VOPc^A (Fig. S4a) and VOPc^B (Fig. S4b). Before annealing, TiOPc molecules in the 1st layer are 4-fold symmetrical, but after annealing and creation of VOPc^B, some of the TiOPc molecules around VOPc^B are elongated along the lobe direction, showing the 2-fold symmetry.

2.3 Geometric Structure of TiOPc on TiOPc Monolayer

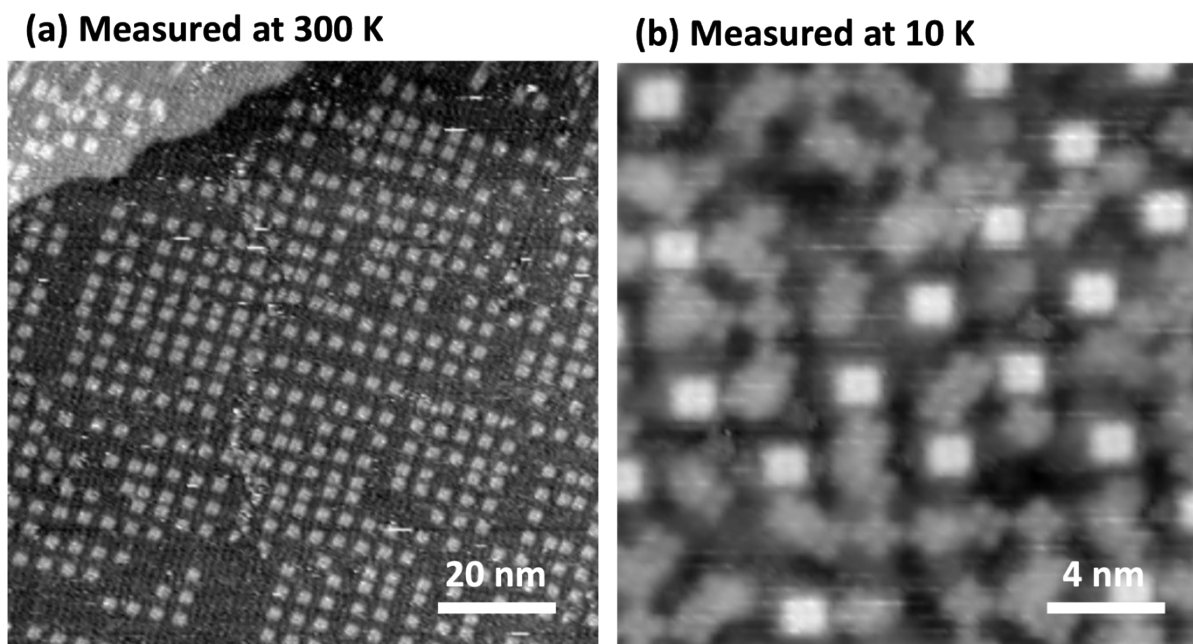


Figure S5. STM topography of sub-ML TiOPc on TiOPc ML after post annealing at 540 K. (a) Large scale STM topography of well-organized TiOPc^B-like molecules measured at room temperature (scan parameters: $V_{DC} = 100$ mV, $I_{set} = 100$ pA, image size: 100×100 nm²). (b) Close-up image of the same sample with (a) measured at 10 K (scan parameters: $V_{DC} = 0.5$ V, $I_{set} = 100$ pA, image size: 20×20 nm²)

We prepared a sub-ML TiOPc on 1 ML TiOPc in the same condition with the sample in Fig. 1(d) of the main text. Figures S5a and S5b show STM images of TiOPc molecules on 1 ML TiOPc/Ag(100) after post-annealing at 540 K as measured at 300 K and 10 K, respectively. Similarly to the VOPc/TiOPc/Ag(100) system shown in Fig. 1 of the main text, we observe a well-organized arrangement of the 2nd molecular layer after annealing. When the sample is measured at 300 K (Fig. S5a), only B-type molecule with long range ordering is observed, and A-type molecules are invisible, suggesting that A-type molecules have higher mobility, while B-type molecules are strongly anchored to the surface even at room temperature.

3. Additional X-ray Absorption Data and Multiplet Calculations

3.1 Background Subtraction Procedure

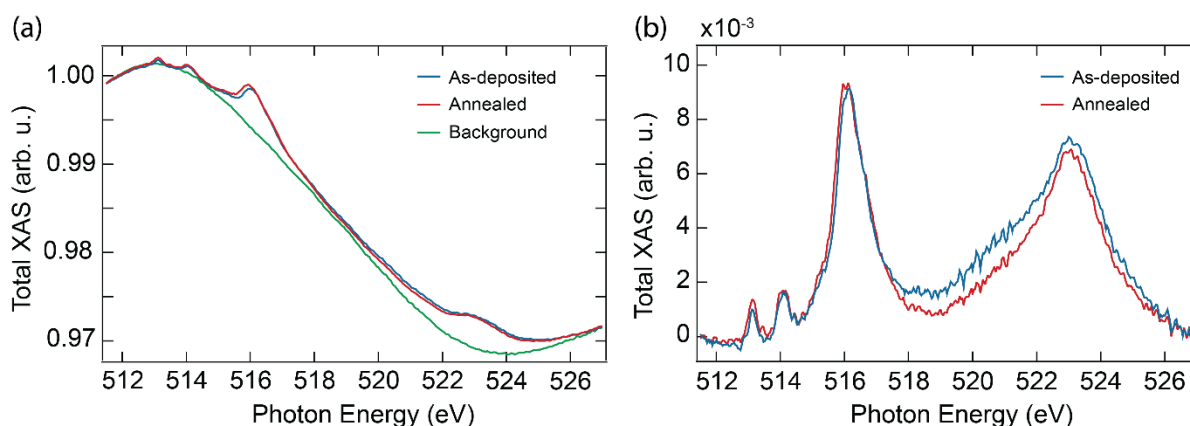


Fig. S6. Comparison of X-ray circular absorption spectra of as-deposited and annealed 0.25 ML VOPc/1.15 ML TiOPc/Ag(100). Summed XAS ($C^+ + C^-$) at the V L_{2,3} edges (a) before and (b) after subtracting the Ag background signal (green solid line). The Ag background was acquired prior to the deposition of the molecular layer and identically subtracted from the XAS spectra acquired on the sample covered with the molecular film ($T = 2.5$ K, $B = 6.8$ T, normal incidence). All XAS data are reported as relative intensities over the background at the pre-edge value.

Figure S6 illustrates the background subtraction procedures that have been followed to present all XAS data in this work. Figure S6a shows the original XAS signal at the V edge for the two spectra presented in Fig. 2a, together with the background signal acquired prior to the molecule deposition on the bare Ag(100) substrate. The intense oscillating background originates from the extended X-ray absorption fine structure (EXAFS) of the Ag M_{45} edges (green line), on top of which the less intense signal of the V absorption is visible for both as-deposited (blue line) and annealed sample (red line). On the original data, the intensity of the signal from the samples covered with molecular films is extremely similar. However, a more precise comparison can be made after the background subtraction, which renders the V signal more clearly visible, see Fig. S6b. The background, being identically subtracted from the two signals, preserves the relative intensities of the peaks. After the subtraction, the two spectra show identical peaks at the L₃ edge (513–518 eV), while a slight difference is visible in the intensity between the two edges, which also extends over the L₂ edge (520–525 eV). The

broad range where the difference is visible suggests that its origin might be due to a change of the EXAFS signal of the Ag substrate, possibly related to minute amount of adsorbates accumulated on the surface after the extended measurement and preparation procedure. These data confirm the absence of V demetallation from the molecular film after the thermal annealing.

To finally produce the comparison of the XAS signals with simulated spectra from multiplet calculations such as those shown in Fig. 2a and in Fig. S7 (see further in the text), we subtract a second-degree function to the spectra, together with a double step baseline (with the steps positioned at the maxima of the $L_{2,3}$ edges, respectively) to remove the contribution of the XAS transitions to the continuum of the free-electron states. This additional subtraction procedure is required as this absorption process is not included in the multiplet calculations.

3.2 Details of Multiplet Calculations

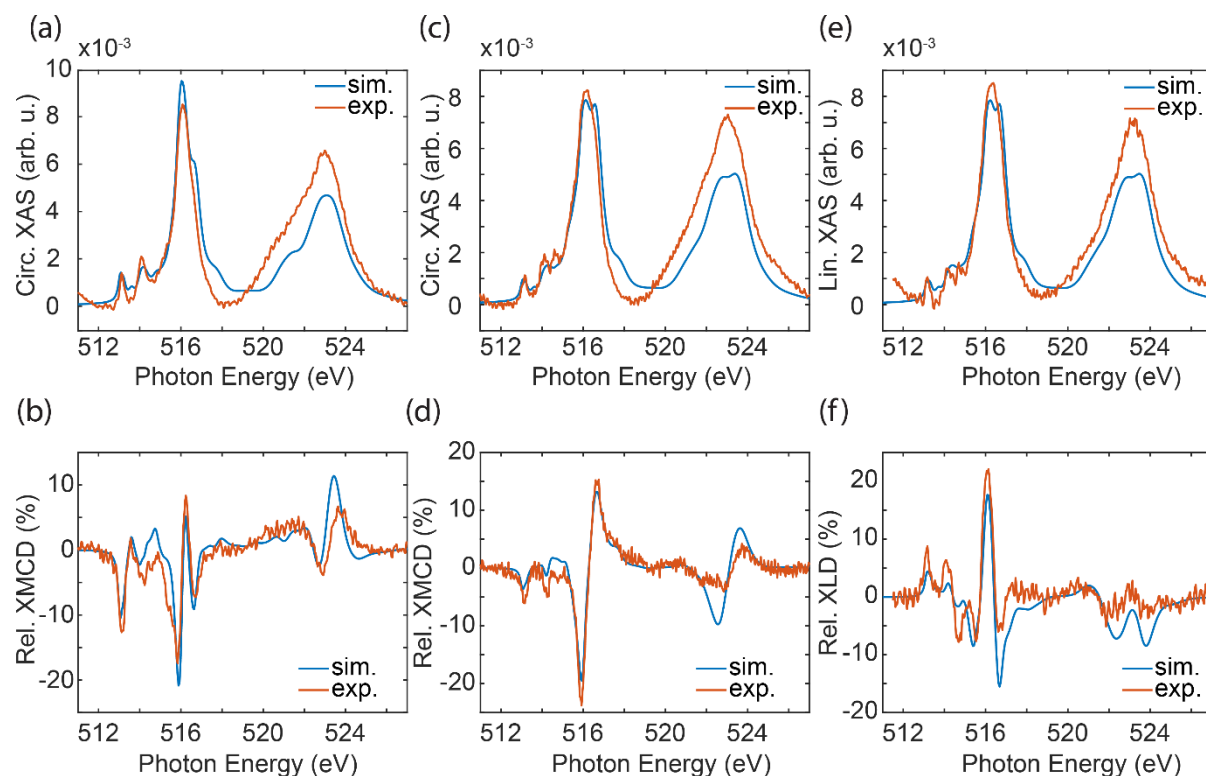


Figure S7. Fit of the V $L_{2,3}$ X-ray absorption spectra using multiplet calculations. (a) Background-subtracted circular XAS and (b) XMCD acquired in normal incidence ($T = 2.5$ K, $B = 6.8$ T). (c) Background-subtracted circular XAS and (d) XMCD at the V $L_{2,3}$ edge acquired in grazing incidence, i.e. with the incident beam and applied field at 60 degrees off from the surface normal ($T = 2.5$ K, $B = 6.8$ T). As described in the main text, the circular XAS is the sum of the two circular right (C^+) and left (C^-) photon polarizations, while the XMCD is the difference of the two ($C^+ - C^-$). (e) Background-subtracted linear XAS and (f) linear dichroism (XLD) obtained in grazing incidence ($T = 2.5$ K, $B = 6.8$ T). The linear XAS is the sum of the two linear horizontal (L^H) and vertical (L^V) polarizations defined with respect to the sample surface (see inset of Fig. 2c). The XLD is the difference between L^H and L^V ($T = 2.5$ K, $B = 0.05$ T). All XAS data are reported as variation of the intensity over the background at the pre-edge value, while XMCD and XLD are shown as percent over the total XAS signal. In all panels, experiments (red solid lines) are shown together with the best fit from multiplet calculations (blue lines). The parameters of the fit obtained from the Bayesian optimization are indicated in Table S1 (In all spectra, coverage of VOPc = 0.25 ML)

Res. $2p-3d$	Res. $3d-3d$	$d_{x^2-y^2}$	d_{z^2}	$d_{xz,yz}$	Amplitude
0.55	0.6	2.40 eV	2.95 eV	2.22 eV	0.00458

Table S1. Best fit parameters for multiplet calculations from Bayesian optimization. The rescaling factor of the $2p-3d$ and $3d-3d$ Slater integrals are applied to the atomic values obtained from the Cowan code.³ The on-site energies for the $3d$ orbitals are reported relative to the lowest d_{xy} orbital. An overall amplitude coefficient is applied to all simulated spectra to match the experiment.

Figure S7 shows the comparison between experiments and spectra from multiplet calculations obtained using the parameters shown in Table S1. From the result of the fit, we infer a crystal field acting on the V electrons that split the $3d$ orbitals by 2.4 to 3 eV from the lowest d_{xy} orbital. These values are in line with our DFT calculation. The obtained reduction factors of the atomic values of the Slater integrals are rather strong with respect to typical values used for transition metals.¹⁴ These values could suggest a possible shortcoming of the crystal field model, that require unusual rescaling of the atomic values of the Slater integrals to match the experiment line shape. The use of a more detailed description of the orbital structure, i.e., using configuration interaction approach, might improve the accuracy of the fit and possibly give a more accurate rescaling value for the adopted Slater Integrals.

3.3 Additional X-ray Data

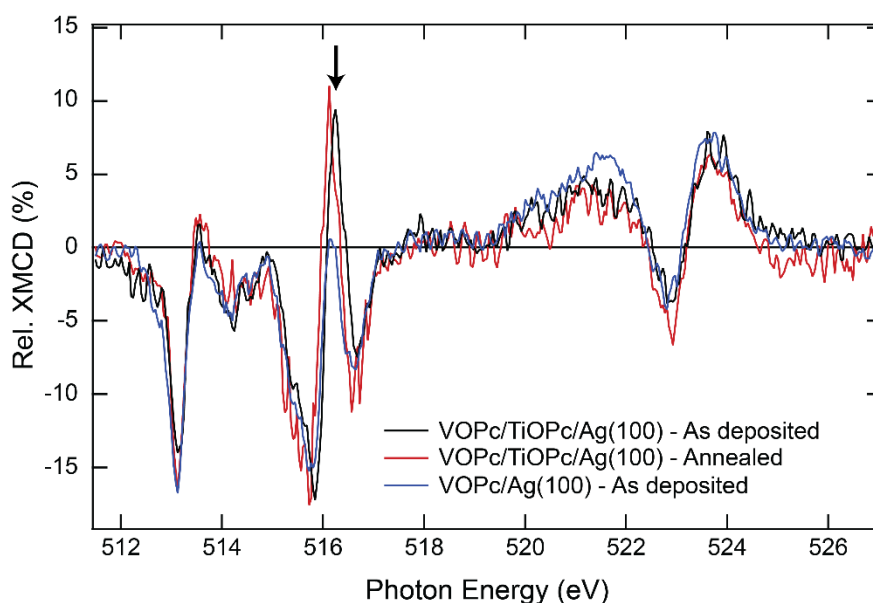


Figure S8. XMCD at the V $L_{2,3}$ edge acquired on 0.7 ML VOPc/Ag(100) and on 0.25 ML VOPc/1.1 ML TiOPc/Ag(100) systems. To compare the spectral features of these samples with different VOPc coverage, the spectra have been normalized to match the amplitude of the XAS at the L_2 edge and expressed as percent over the total XAS signal. The spectral feature at 516.2 eV indicated by the arrow distinguishes the VOPc molecules in direct contact with the metal from those decoupled through the TiOPc layer ($B = 6.8$ T, $T = 2.5$ K). The XMCD spectra of VOPc/TiOPc/Ag(100) are the same as those shown in Fig. 2b of the main text.

To rule out possible intermixing between VOPc and TiOPc layers after annealing, we compare the XMCD at normal incidence for a sub-ML VOPc directly deposited on Ag(100) with the data of the VOPc/TiOPc/Ag(100) shown in the main text before and after the annealing at 540 K (Fig. S8). Despite the similarities between the XMCD spectra of the three systems, the intensity of the spectral feature at 516.2 eV is quite different between the pristine VOPc/Ag(100) and VOPc/TiOPc/Ag(100). This feature provides a clear way to identify whether the VOPc molecules are in contact with Ag or decoupled from it through the TiOPc layer. As we observe no changes in the intensity of this feature after annealing the VOPc/TiOPc/Ag(100) system, we can rule out any significant migration of VOPc molecules to the bottom layer. This evidence, combined with the absence of variation of the amount of

top layer molecules before and after annealing, allows us to also exclude migration of the TiOPc to the top layer.

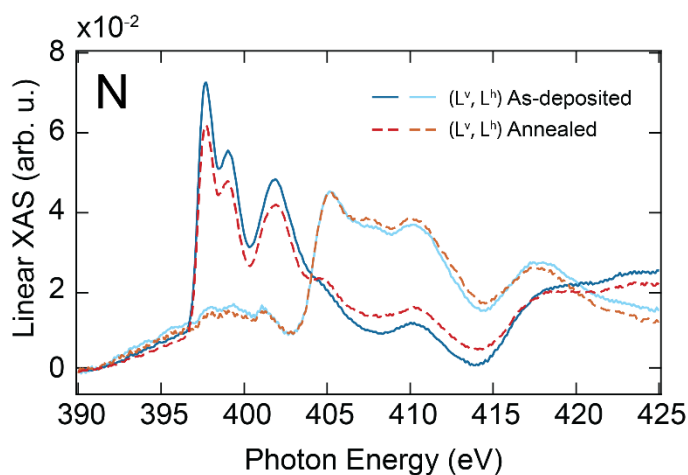


Figure S9. Comparison of linear XAS of as-deposited and annealed 0.25 ML VOPc/1.15 ML TiOPc/Ag(100). The near-edge linear XAS at the N K edge shows individual vertical (L^v) and horizontal (L^h) polarization signals ($T = 300$ K, $B = 0.05$ T, 60 degrees grazing incidence). All XAS data are reported as variation of the intensity over the background at the pre-edge value.

The linear XAS data on N K edge shown in Fig. S9 follow the same behavior observed for the C K edge (Fig. 2c of the main text). Upon annealing at 540 K, the signal at the π^* orbitals detected in the L^v polarization decreases and part of the K edge intensity is redistributed in the spectral region characteristic of the σ^* bonds, further supporting the interpretation of a reduced molecular planarity of the TiOPc molecular layer. The absence of changes in the XAS of Ti $L_{2,3}$ (Fig. S10a and S10b) and in the XAS of V $L_{2,3}$ and O K edges (Fig. S10d and S10e) upon annealing allows us to exclude chemical modifications such as demetallation and detachment of the apical oxygen from the molecules. No variations have been observed on the XLD of V and O (Fig. S10f), while slight reduction of the XLD in several spectra regions (see Fig. S10c) may be due to the reduced planarity of the TiOPc induced by the stress in the molecular layer after the formation of VOPc^B molecules, as discussed in the main text.

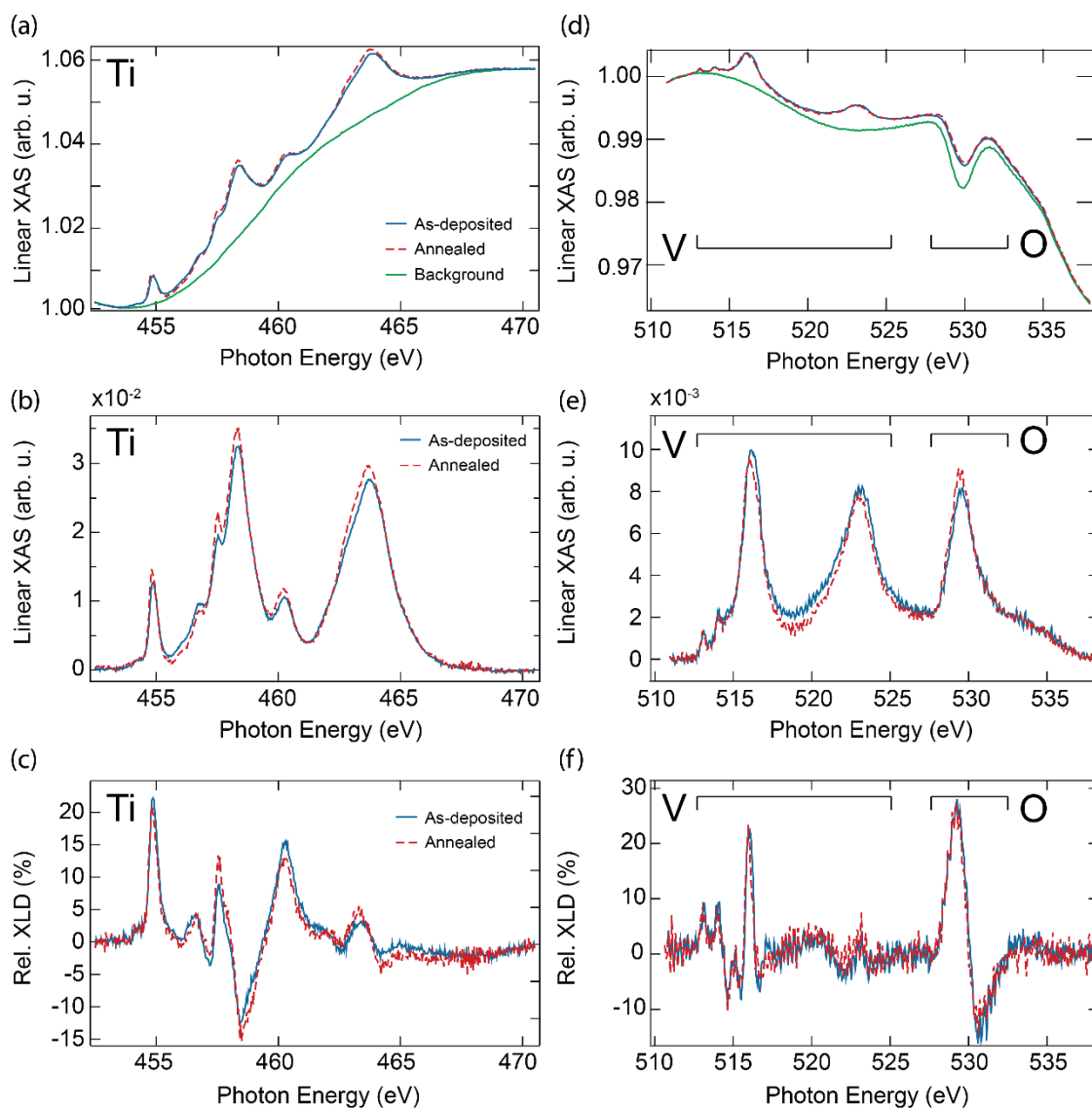


Fig. S10. Comparison of linear XAS of as-deposited and annealed 0.25 ML VOPc/1.15 ML TiOPc/Ag(100). Summed XAS ($L^h + L^v$) at the Ti $L_{2,3}$ edges (a) before and (b) after subtracting the Ag background signal (green solid line). The Ag background was acquired prior to the deposition of the molecular layer and identically subtracted from the XAS spectra acquired on the sample covered with the molecular film. (c) XLD ($L^h - L^v$) at the Ti $L_{2,3}$ edges. Summed XAS at the V $L_{2,3}$ and O K edges (d) before and (e) after subtracting the Ag background signal. (f) XLD at the V $L_{2,3}$ and O K edges ($T = 300$ K, $B = 0.05$ T, 60 degrees grazing incidence). All XAS data are reported as relative intensities over the background at the pre-edge value, while XLD data are shown as percent over the background subtracted XAS signal.

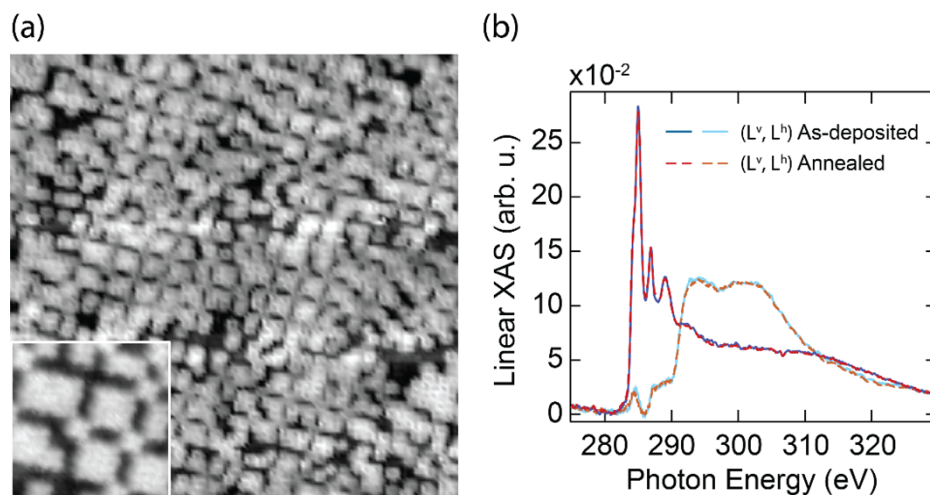


Figure S11. Carbon K edge for larger coverage of VOPc. (a) STM topography of 60% coverage of VOPc on 1 ML TiOPc on Ag(100), which was post-annealed at 540 K (scan parameters: $V_{DC} = 1.0$ V, $I_{set} = 100$ pA, $T = 10$ K, scan size: 60×60 nm²; inset: $V_{DC} = 0.5$ V, $I_{set} = 100$ pA, $T = 10$ K, scan size: 10×10 nm²) (b) Linear XAS at the C K edge for 0.6 ML of VOPc on 1.1 ML TiOPc layer ($T = 300$ K, $B = 0.05$ T, grazing incidence). All XAS data are reported as variation of the intensity over the background at the pre-edge value.

Figure S11a shows an STM image of 0.6 ML of VOPc deposited on top of TiOPc/Ag(100) after annealing at 540 K. Differently from what observed for samples with lower VOPc coverage, the annealing has no effect on the molecular types, *i.e.* we do not observe any VOPc^B molecules on the top layer. Conversely, the VOPc^A types arrange in a more closely packed array, where squared/rectangular blocks of 4 or more molecules repeat periodically, together with individual molecules connecting the corners of blocks (inset in Fig. S11a). In contrast to what we observed for samples with a lower coverage of VOPc (Fig. 2 of the main text), the C K edge XAS of a sample with 0.6 ML VOPc on TiOPc/Ag(100) reveals no difference between as-deposited and annealed molecular films, see Fig. S11b. This evidence supports the conclusion that the changes in the C K edge shown in Fig. 2c of the main text are related to the formation of VOPc^B molecules.

4. Additional dI/dV Spectra and DFT Calculations

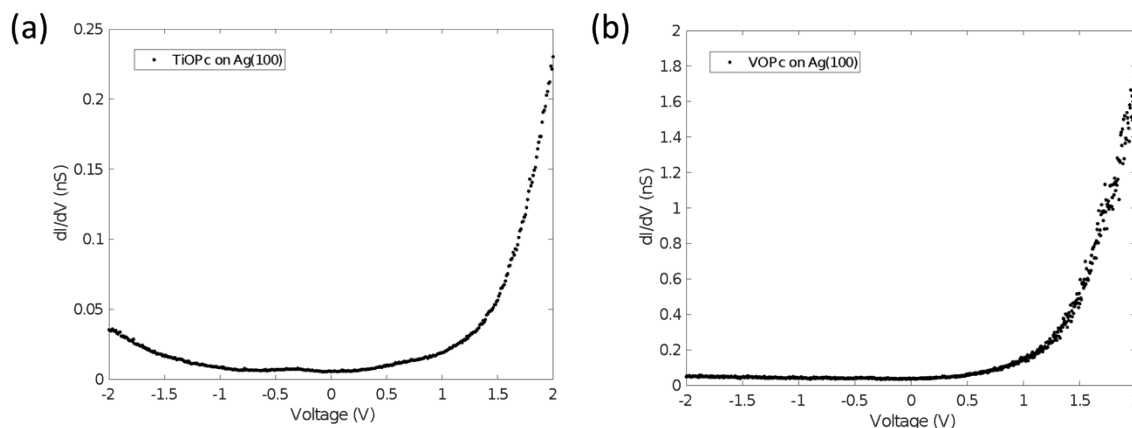


Figure S12. Electronic properties of a single TiOPc and VOPc molecule directly on Ag(100) surface. (a) dI/dV curve of the single TiOPc molecule on Ag(100) ($V_{DC} = 0.7$ V, $I_{set} = 100$ pA, $V_{mod} = 10$ mV). (b) dI/dV curve of the single VOPc molecule on Ag(100) ($V_{DC} = 0.5$ V, $I_{set} = 50$ pA, $V_{mod} = 15$ mV).

To reveal the electronic property of the TiOPc and VOPc molecules directly sitting on the metal substrate, we measured dI/dV spectra of TiOPc and VOPc molecules on Ag(100). The curve measured on TiOPc (Fig. S12a) shows a relatively flat density of states (DOS) at -2 V to 1.5 V with a large slope over 1.5 V. A small peak at -0.3 V originates from the tip, as it is appearing in spectra taken on the bare Ag surface. Similarly, the curve measured on VOPc (Fig. S12b) shows flat DOS below 1.5 V without any distinct molecular features, suggesting the molecular orbital peaks are largely broadened by the strong coupling between VOPc molecules and electrons from Ag.

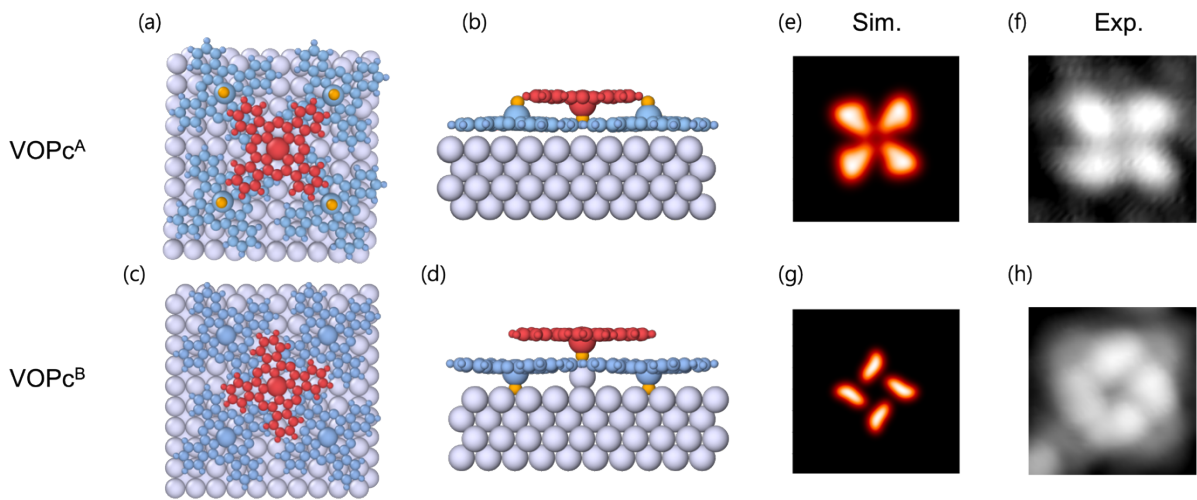


Figure S13. Top, and lateral view of the unit cell corresponding at (a,b) VOPc^A and (c,d) VOPc^B respectively. The first ML of TiOPc is presented in blue while the VOPc molecule is in red. To improve the visualization of the molecular orientation, O atoms are colored in orange. (e, f) and (g, h) are simulated and experimental topographic images of VOPc^A and VOPc^B, respectively. To highlight the difference between the electronic properties of the two configurations, we show both systems at a sample bias located in the VOPc^A energy gap, which instead corresponds to a molecular state in the VOPc^B (scan parameters: (e) and (g) $V_{DC} = -0.1$ V, scan size: 1.44×1.44 nm², (f) and (h) $V_{DC} = 0.5$ V, $I_{set} = 100$ pA, scan size: 2×2 nm²).

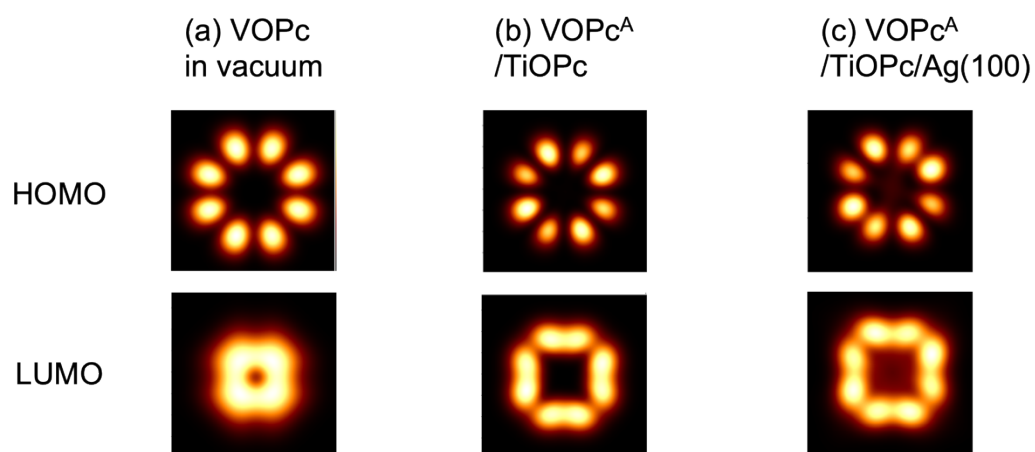


Figure S14. Simulated dI/dV images of highest occupied molecular orbital (HOMO) and lowest unoccupied molecular orbital (LUMO) of a free-standing VOPc molecule in vacuum, VOPc molecule on TiOPc layer, and VOPc molecule on TiOPc/Ag(100).

From the comparison between the simulated dI/dV images of HOMO and LUMO for the different geometries (Fig. S14), we see that there are no major changes. On the other hand if we compare the composition of LUMO and HOMO as shown in Table S2 we see that the difference between the values of the different systems is less than 1%. Both results are in agreement with the idea that 1 ML TiOPc decouples the VOPc molecule from the metal substrate.

System	Energy (eV)	VOPc Composition (%)	
	(HOMO – LUMO)	C HOMO/LUMO	N HOMO/LUMO
VOPc Vacuum	-1.36	99/68	-/28
VOPc ^A /TiOPc	-1.38	96/66	-/28
VOPc ^A /TiOPc/Ag(100)	-1.27	95/42	-/20
VOPc ^B /TiOPc	-1.4	95/66	-/25
VOPc ^B /TiOPc/Ag(100)	-1.35	93/55	-/20

Table S2. Calculated HOMO and LUMO energy levels and its carbon and nitrogen compositions for VOPc in different environments. The energy levels are relative to the LUMO.

All the simulations for VOPc^B are done with 35-degree rotation with respect to the molecular unit cell vector, which is 11 degrees more rotated from the experimentally determined value from STM images. 35-degree rotated geometry has the lowest energy from the DFT after relaxation, but the difference between two systems is 0.06 eV. To rule out changes in the electronic structure induced by azimuthal rotations of the molecule, we compare the DOS of two configurations (Fig. S15), and pDOS of two systems shows no difference in the range of -2 V to 2 V, which corresponds to the bias voltage used in the experiment.

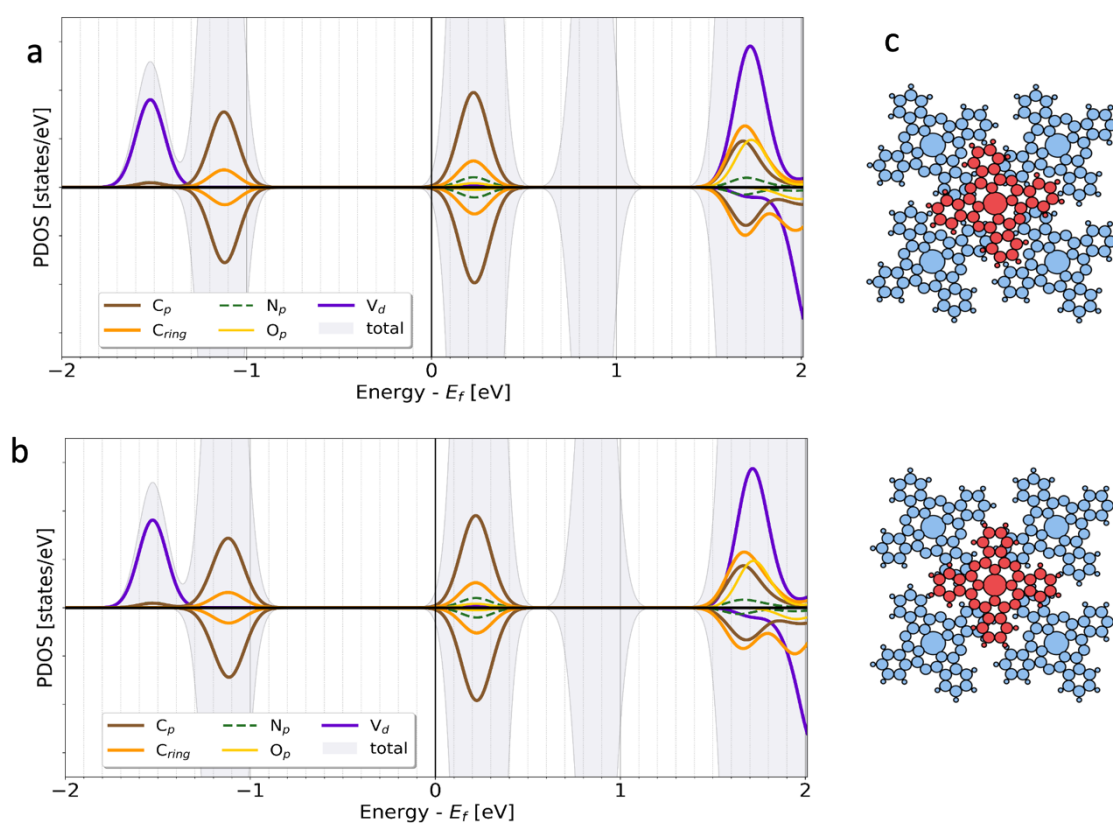


Figure S15. Comparison of pDOS of VOPc^B/TiOPc at different azimuthal angles. (a) VOPc^B/TiOPc and (b) VOPc^B molecule rotated by 11 degrees clockwise with respect to one in (a). The Fermi level is set at zero energy. (c) Schematic representations of the adsorption configurations for each calculation.

REFERENCES

1. C. Piamonteze, U. Flechsig, S. Rusponi, J. Dreiser, J. Heidler, M. Schmidt, R. Wetter, M. Calvi, T. Schmidt, H. Pruchova, J. Krempasky, C. Quitmann, H. Brune and F. Nolting, *J Synchrotron Radiat*, 2012, **19**, 661-674.
2. M. W. Haverkort, *Journal of Physics: Conference Series*, 2016, **712**, 012001.
3. R. D. Cowan and U. o. C. Press, *The Theory of Atomic Structure and Spectra*, University of California Press, 1981.
4. M. W. Haverkort, *J. Phys.: Conf. Ser.*, 2016, **712**, 012001.
5. M. O. Krause and J. H. Oliver, *J. Phys. Chem. Ref. Data*, 1979, **8**, 329-338.
6. P. Giannozzi, S. Baroni, N. Bonini, M. Calandra, R. Car, C. Cavazzoni, D. Ceresoli, G. L. Chiarotti, M. Cococcioni, I. Dabo, A. Dal Corso, S. de Gironcoli, S. Fabris, G. Fratesi, R. Gebauer, U. Gerstmann, C. Gougoussis, A. Kokalj, M. Lazzeri, L. Martin-Samos, N. Marzari, F. Mauri, R. Mazzarello, S. Paolini, A. Pasquarello, L. Paulatto, C. Sbraccia, S. Scandolo, G. Sclauzero, A. Seitsonen, A. Smogunov, P. Umari and R. M. Wentzcovitch, *J. Phys.: Condens. Matter*, 2009, **21**, 395502.
7. P. Giannozzi, O. Andreussi, T. Brumme, O. Bunau, M. Buongiorno Nardelli, M. Calandra, R. Car, C. Cavazzoni, D. Ceresoli, M. Cococcioni, N. Colonna, I. Carnimeo, A. Dal Corso, S. de Gironcoli, P. Delugas, R. A. DiStasio, A. Ferretti, A. Floris, G. Fratesi, G. Fugallo, R. Gebauer, U. Gerstmann, F. Giustino, T. Gorni, J. Jia, M. Kawamura, H. Y. Ko, A. Kokalj, E. Küçükbenli, M. Lazzeri, M. Marsili, N. Marzari, F. Mauri, N. L. Nguyen, H. V. Nguyen, A. Otero-de-la-Roza, L. Paulatto, S. Poncé, D. Rocca, R. Sabatini, B. Santra, M. Schlipf, A. P. Seitsonen, A. Smogunov, I. Timrov, T. Thonhauser, P. Umari, N. Vast, X. Wu and S. Baroni, *J. Phys.: Condens. Matter*, 2017, **29**, 465901.
8. A. Dal Corso, *Comput. Mater. Sci.*, 2014, **95**, 337-350.
9. J. P. Perdew, K. Burke and M. Ernzerhof, *Phys. Rev. Lett.*, 1996, **77**, 3865-3868.
10. R. Sabatini, T. Gorni and S. de Gironcoli, *Physical Review B*, 2013, **87**, 041108.

11. S. Colonna, G. Mattioli, P. Alippi, A. Amore Bonapasta, A. Cricenti, F. Filippone, P. Gori, A. M. Paoletti, G. Pennesi, F. Ronci and G. Zanotti, *The Journal of Physical Chemistry C*, 2014, **118**, 5255-5267.
12. N. L. a. R.Robles, 2019, DOI: <https://zenodo.org/record/3581159>.
13. <https://github.com/qphensurf/STMpw-QuantumEspresso>.
14. F. d. Groot, *Coord. Chem. Rev.*, 2005, **249**, 31-63.